Direct Observation of Charge Transfer and Magnetism in Fe4 Co4 Cyanide-Bridged Molecular Cubes

Niéli Daffé, Marie-Anne Arrio, Juan-Ramón Jiménez, Michal Studniarek, Amina Benchohra, Rodrigue Lescouëzec, Jan Dreiser

Direct Observation of Charge Transfer and Magnetism in Fe_4Co_4 Cyanide Bridged Molecular Cubes

Niéli Daffé,[§,*] Juan-Ramón Jiménez,[¥] Michał Studniarek,[§] Amina Benchohra,[¥] Marie-Anne Arrio,[£] Rodrigue Lescouëzec,[¥] and Jan Dreiser[§,*]

§ Paul Scherrer Institut, CH-5232 Villigen PSI, Switzerland

¥ Institut Parisien de Chimie Moléculaire, CNRS UMR 8232, Sorbonne Université, FR-75252 Paris cedex 05, France

£ Institut de Minéralogies, Physiques des Matériaux et de Cosmologie, CNRS UMR 7590, Sorbonnes Universités, FR-75252 Paris cedex 05, France

Corresponding authors:

*Email Addresses: nieli.daffe@psi.ch, jan.dreiser@psi.ch

ABSTRACT

We have studied the zero-dimensional cubane molecular correspondent of a Prussian blue analogue Cs-Fe_4Co_4 at low temperature and high magnetic field by means of L-edge X-ray absorption spectroscopy and X-ray magnetic circular dichroism. We probe the magnetic and electronic structures of Fe and Co separately upon light irradiation, which allows us to observe directly the electron transfer coupled to a spin transition (ETCST) phenomenon within the molecular cubes and to investigate the nature of the metastable photoexcited state. From our results we estimate a lower bound for the intramolecular Fe-Co exchange coupling of $J \gtrsim -0.5\ \mathrm{cm}^{-1}$ with the negative sign denoting antiferromagnetic coupling.

TOC GRAPHICS.

KEYWORDS. Photomagnetism, Prussian blue analogues, Charge transfer, Cyanometalates, XMCD, XAS

The photocontrol of the magnetic and optical properties of switchable compounds is of great interest in view of possible implementations as sensors, optical switches or memories in organic electronics devices.[1–7] FeCo Prussian Blue Analogues[8] (PBAs) are excellent candidate materials exhibiting a photoinduced metastable state as reported in the inorganic $K_{0.2}Co_{1.4}[Fe(CN)_6]\cdot 6.9H_2O$ PBA.[9] At the origin of the substantial changes of the magnetic properties in these three-dimensional networks of metallic ions connected by cyanide ligands, there is a metal-to-metal electron transfer within the Fe-CN-Co pairs associated with a spin transition of the Co ions, known as the electron transfer coupled to spin transition (ETCST) phenomenon.[10,11] The ground state is formed from pairs of Co and Fe ions both in the t_{2g}^6 configuration. After the ETCST, in the excited state the formerly diamagnetic (Co^{III}, t_{2g}^6, S = 0) − (Fe^{II}, t_{2g}^6, $S = 0$) pairs are converted to the paramagnetic (Co^{II}, t_{2g}^5 e_g^2, $S = 3/2$) − (Fe^{III}, t_{2g}^5, S = 1/2) ones. A schematic representation of the ETCST process in FeCo 3D-PBA is depicted Figure 1a.

Lately, cyanide-bridged FeCo systems have attracted a renewed attention when the light-induced magnetic properties of PBAs were successfully transferred to discrete molecular FeCo models. First demonstrations include the report of thermally-induced ETCST in a Fe_2Co_3 pentanuclear complex[12] and the photomagnetic effect in a zero-dimensional molecular cube of Fe_4Co_4 was reported for the first time a decade ago.[13] Since then, the many advantages of transferring the photomagnetic properties to zero-dimensional molecular systems were corroborated.[14–20] These include less structural complexity than in 3D-PBAs facilitating rationalization and optimization of their magnetic properties, the availability of single crystals and good solubility. Similar to 3D-PBA, the light-induced properties of the molecular systems are also attributed to the mechanism of ETCST.

The characterizations of the metal-to-metal electron transfer processes are typically performed indirectly using magnetometry or X-ray structural analysis. In this respect, X-ray absorption spectroscopy (XAS) is a very powerful technique able to clarify the electronic structure of transition metals, including valence and spin states and crystal-field splitting by a direct observation of the 2p → 3d dipole allowed transitions at the $L_{2,3}$ edges. The technique has been indeed successfully applied to examine the light-induced excited spin state trapping (LIESST) in spin-crossover complexes and PBA.[21–24] The direct observation of the ETCST properties to the photomagnetic molecular complexes was reported by Sekine *et al.* who have investigated the thermal and X-ray induced conversion in Fe_2Co_2 cyanide bridge molecular squares using K-edge XAS.[25] Very recently, Fatima *et al.* have evidenced the occurrence of the thermal and light-induced electron transfer in a FeCo dinuclear complex using L-edge XAS and XMCD electron transfer.[26] Another important unknown is the nature of the Fe-Co magnetic coupling in the photoinduced paramagnetic state of the molecular systems. While in 3D-PBA an antiferromagnetic coupling between the Co^{II}_{HS} and the Fe^{III}_{LS} was reported,[27] calculations on paramagnetic 1D FeCo chains[28] and on 0D FeCo square complexes[29] have demonstrated that intramolecular ferromagnetic exchange pathways may dominate in the lower dimensional systems.

In this study, we employ L-edge XAS and X-ray Magnetic Circular Dichroism (XMCD) to examine the photomagnetic process in the discrete molecular heterocubane $Cs\subset\{[Fe^{II}(Tp)(CN)_3]_4[Co^{III}(^{pz}Tp)]_3[Co^{II}(^{pz}Tp)]\}\cdot 12CH_3CN$ cluster[30] (Tp = hydrotris(pyrazol-1-yl)borate; ^{pz}Tp = tetra(pyrazol-1-yl)borate), from here on referred to as Cs-Fe_4Co_4. This system is the true zero-dimensional model of the Cs-FeCo 3D-PBA. Besides, the remarkable stability of these cubic molecules in solution allows to envision different solution processes for the surface

deposition of these materials, which is of extreme importance for applications in molecular electronics or spintronics devices. Taking advantage of the elemental selectivity of XAS, we follow the changes of the electronic structure of Fe and Co upon photoexcitation proving the concurrent electron transfer between these ions as well as the Co spin state change. Furthermore, we resolve the exact compositions of the ground state and of the metastable excited state with the support of ligand-field multiplet (LFM) calculations. To the best of our knowledge, we report for the first time an XMCD study of the photoinduced-excited state in a Fe_4Co_4 cubane system. We exploit the magnetic sensitivity of XMCD as a local probe of the magnetic moments of the Fe and Co ions and to obtain insight into the magnetic coupling between the metallic centers in Cs-Fe_4Co_4.

The neutral cyanide-bridged Fe_4Co_4 cage encapsulating a Cs^+ ion is depicted in **Figure 1b.** Details about the synthesis, magnetic and structural characterization of Cs-Fe_4Co_4 can be found in ref. 30.

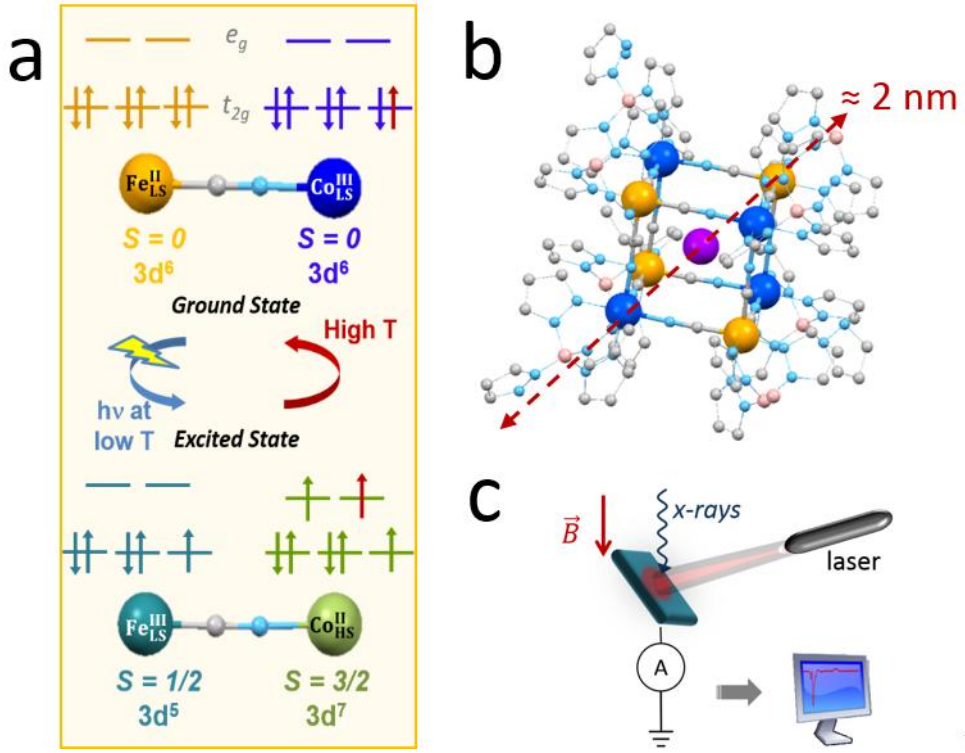

Figure 1. (a) Schematic representation of the ETCST process in FeCo 3D-PBA. (b) Scheme of the XAS and XMCD experimental geometry (c) Ball-and-stick representation of Cs-Fe_4Co_4. Hydrogen atoms, solvent molecules, and Cs bonds are omitted for clarity. Color code: iron: orange, cobalt: blue, cesium: purple, nitrogen: light blue, carbon: grey, boron: pink. The scale bar has a length of XXX nm.

A solution of Cs-Fe_4Co_4 in dichloromethane ($c \sim 1$ mM) was sprayed onto a gold-coated silicon substrate to obtain a homogeneous and clearly visible film of molecular deposit after the evaporation of the solvent indicating a film thickness much larger than the probing depth of the total electron yield (TEY) detection of a few nanometers. No additional capping was used and a comparison of the XAS recorded on a polycrystalline sample revealed that the molecules are fully intact in the film (Supporting Information **Figure S1**). These findings are consistent with the stability of the molecules in solutions as demonstrated in ref. 30. XAS and XMCD spectra were recorded at the X-Treme beamline of the Swiss Light Source.[31] The sample was positioned so that the X-ray beam was incident at an angle of 30° from the sample surface as depicted in **Figure 1c**. XAS measurements were performed in total electron yield (TEY) mode with the

magnetic field applied parallel to the beam propagation direction. A large spot size (0.5 × 2.5 mm^2) and a low photon flux were chosen to avoid radiation damage. The spectra were normalized to the maxima of the Fe or Co L_3 edges after subtraction of the background using a step function to allow a direct comparison with the simulations. A laser (λ = 650 nm) with moderate intensity of ~1 mW/mm² was used to photoexcite the molecules for a total of 3 hours.

Fe and Co XAS recorded at 300 K before the irradiation and at 2 K after the laser irradiation are shown in **Figure 2**. Initially, the Fe L_3 edge exhibits a double-peak shape. After laser irradiation at 2 K, additional features appear including a broad shoulder at around 710.9 eV and a sharp peak at the lower energy of 705.8 eV. The Co L_3 edge displays one main peak at 779.7 eV and smaller contributions at 775.5 eV, 776.9 eV and 778.3 eV before laser irradiation. In contrast, after irradiation the contributions of features at lower energies prevail, while the peak at 779.7 eV is significantly reduced. Upon heating the sample to 300 K after the laser irradiation at low temperature relaxes the molecules to the ground state, since the molecules are trapped in the photoexcited state only up to a few tens of Kelvin. The ground state of Cs-Fe_4Co_4 is fully recovered as shown by the substantial overlap of the spectra acquired after warming up the sample and the ones recorded before irradiation at low temperature in **Figure 2**. The thermal reversibility which we evidenced by XAS is in good agreement with previous SQUID measurements described in ref 28. Furthermore, it testifies to the absence of damage of the sample by the laser and X-ray irradiation.

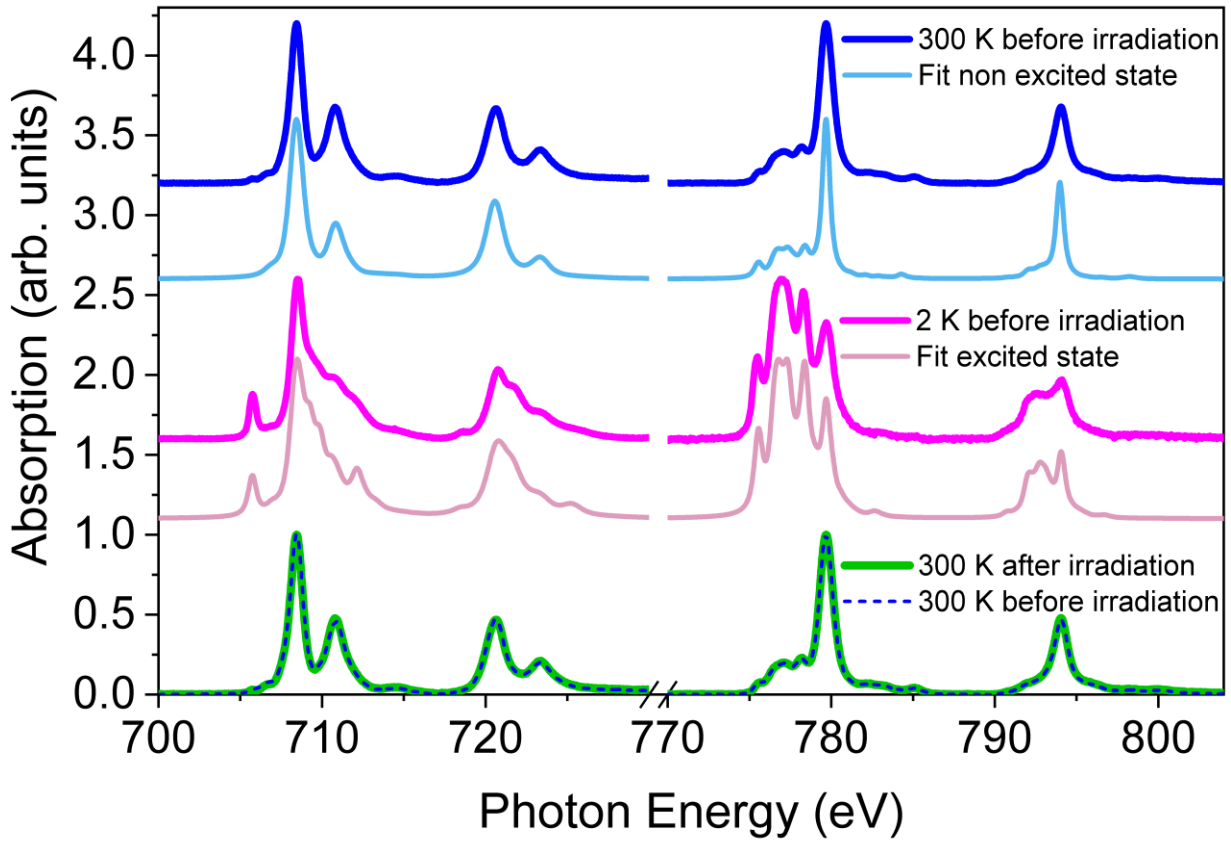

Figure 2. Experimental XAS of the ground and excited states measured at the Fe $L_{2,3}$ edges (700 eV – 740 eV) and Co $L_{2,3}$ edges (770 eV- 805 eV) of Cs-Fe_4Co_4 and calculated best-fit curves. All fits exhibit a high coefficient of determination $0.81 \leq R^2 \leq 0.95$.

A more precise analysis and understanding of the X-ray spectra of the ground and excited states is obtained by comparison with theoretical spectra of multiplet features of Fe^{III}_{LS}, Fe^{II}_{LS}, Co^{III}_{LS} and Co^{II}_{HS} (LS: low spin and HS: high spin). Spectra were calculated using LFM theory as implemented in the CRISPY software package.[32] In the molecular Cs-Fe_4Co_4 cubes, all metal ions experience a slightly distorted octahedral coordination sphere. with a pseudo C_3 axis along the boron-metal direction. In order to approximate this distorted octahedral environment, the calculations are performed using a C_{3v} point symmetry for the metallic ions and the strength of the crystal field potential is therefore defined using three independent parameters Dq, Dσ and Dτ. Details of the parameters used are given in the Supporting Information (SI). The simulations of

the Fe L-edge spectra were performed in order to match the ones of the mononuclear reference complexes $K_2[Fe^{II}(Tp)(CN)_3]$ and $NBu_4[Fe^{III}(Tp)(CN)_3]$ (see Supporting Information **Figures S2** and **S3** possessing well-known oxidation numbers. The best-fit calculations of the X-ray spectra are presented in **Figure S4**. The best simulation of $K_2[Fe^{II}(Tp)(CN)_3]$ is obtained for Fe^{II} ions with relatively strong cubic crystal field of 2.8 eV consistent with a LS state. To reproduce the spectral shape of Fe^{III}_{LS}, the same parameters reported for the precursor $[TpFe^{III}CN_3]$ by Jafri and co-workers are used (10 Dq = 2.8 eV; $D\sigma$ = 0.07 eV, $D\tau$ = 0.12 eV). The Fe L-edge spectrum measured on Cs-Fe_4Co_4 at 300 K before photoexcitation plotted in **Figure 2** is manifestly very similar to the simulations obtained for Fe^{II}_{LS}. In contrast, the peak at 705.2 eV is the signature of Fe^{III}_{LS}, which is observed in the excited state of Cs-Fe_4Co_4. This peak is known to originate from the $2p^6t_{2g}{}^5 \rightarrow 2p^5t_{2g}{}^6$ transitions that are absent in the Fe^{II}_{LS} configuration.[11]

Concerning the Co spectra, the peaks centered at 775.8 eV, 776.8 eV and 778.2 eV are fingerprints of Co^{II} in a sixfold coordination environment, while the signature of Co^{III} is characterized by peaks at 779.7 eV and 783.1 eV. The features corresponding to Co^{III} are shifted toward higher energies due to the shortening of the Co-ligand bonds as compared to Co^{II}. This well-defined separation in energy allows the comparison of the respective spectral features. The results obtained on the mononuclear reference compounds for Co^{II} and Co^{III} are presented and discussed in the SI **Figure S3**. The contributions of $Co^{II}$are well modeled using the C3v symmetry which takes into account the deviation from the octahedral symmetry because of the non-equivalent ligands. A weak crystal field of 10 Dq = 0.11 eV is found for the Co^{II} ions, in agreement with the axial distortion factor (Δ = -922 cm^{-1}) previously reported and compatible with the expected HS state. In contrast, the best simulation in the case of the Co^{III} ions corresponds to the higher 10Dq potential value of 0.5 eV consistent with a LS state.

The straightforward comparison of typical spectral features of both Fe and Co ions in Cs-Fe_4Co_4 as visible in **Figure 2**, along with the LFM calculations described in the above, yields clear evidence of the occurrence of the light-induced excited state at 2 K. The spectra obtained after irradiation with the laser show an increase of the signatures of Co^{II}_{HS} and Fe^{III}_{LS} compared to the ground state at room temperature, which mainly includes Co^{III}_{LS} and Fe^{II}_{LS}. The signatures of Co^{III}_{LS} and Fe^{II}_{LS} in the excited state do not disappear completely, which indicates that the conversion is not complete for both Fe and Co ions. This is expected because of the initial presence of Co^{II} ions in the ground state which implies the presence of Fe^{II} ions in the excited state.

In order to extract quantitative information about the relative amount of Co^{II}/Co^{III} and Fe^{II}/Fe^{III}, linear combinations presented in **Figure 2** of the modeled spectra are used to visually

fit the measurements obtained for Cs-Fe_4Co_4. We find 100% of Fe^{II}_{LS} and a mix of 16±1% of Co^{II}_{HS} and 84±1 % of Co^{III}_{LS} in the ground state.The amount of Co^{II} in the ground state is lower than the 25% that were previously reported.[30] Due to the probing depth of TEY of a few nanometers, this result can be interpreted in terms of surface oxidation of part of the cubes. The excited state is composed of 52±1 % Fe^{II}_{LS} + 48±1 % Fe^{III}_{LS} on the one hand and 64±1 % of Co^{II}_{HS}+ 36±1 % of Co^{III}_{LS} on the other hand (see SI **Figures S4 and S5**). From the compositions of the ground and excited states we conclude that 48±1 % of Co^{III}_{LS} are transformed into Co^{II}_{HS} while 48±1 % of the initial Fe^{II}_{LS} ions in the ground state are oxidized toward Fe^{III}_{LS} during the three hours of laser irradiation. These findings are perfectly consistent, and they demonstrate the concomitance of the Fe oxidation with the Co reduction. This is further supported by the observation of the XAS changes during the irradiation process. **Figure S5** in the SI shows the comparison of the variation of Co^{II} and Fe^{III} in time during laser irradiation, revealing similar time constants for Co and Fe extracted from monoexponential fits. Altogether, these results show that only a charge transfer between the Fe and the Co ions associated with a Co spin transition can be at the origin of the simultaneous transformation. **Figure S5** indicates that the conversion is not complete after 3 hours of irradiation. This may be due to the 650 nm wavelength deviating from 800 nm for which a full conversion was reported in these compounds,[18] and/or the presence of Co^{II} in the ground state preventing the electron-transfer of 16% of the Co-CN-Fe pairs.

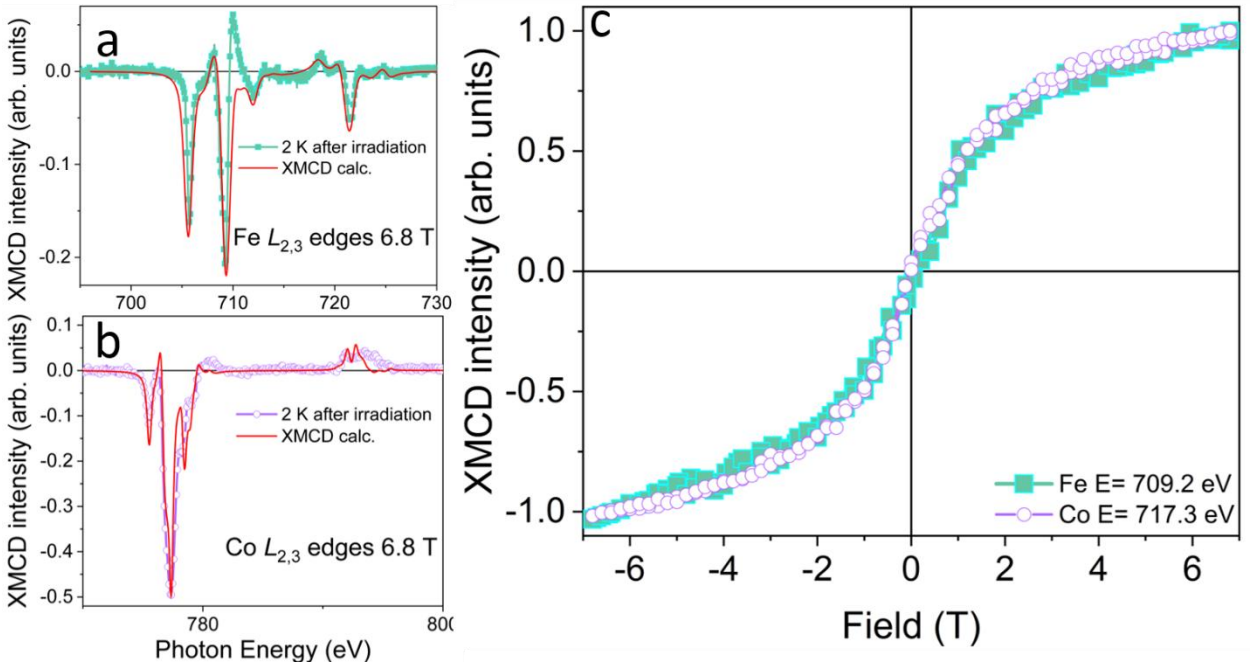

Figure 3. Experimental and calculated XMCD spectra measured after laser excitation at 2 K(a) at the Fe $L_{2,3}$ edges and (b) at the Co $L_{2,3}$ edges in a magnetic field of 6.8 T and at 2 K. Symbols and solid lines denote experimental data and calculations, respectively. (c) Experimental, element specific and normalized $M(H)$ curves extracted from XMCD are plotted as symbols.

Beyond the averaged properties provided by SQUID magnetometry, XMCD helps to determine the local magnetic moments of the ions in the Cs-Fe_4Co_4 cages. XMCD spectra were recorded on the Cs-Fe_4Co_4 ground state at 200 K, well above the relaxation temperature of the system of ca. 66 K (see **Figure S5**). No XMCD signal is detected at 200 K at the Fe $L_{2,3}$ edges. This is consistent with the above conclusion that the ground state contains solely LS Fe^{II}. In contrast, at the Co $L_{2,3}$ edges, a clear dichroic signal of the order of 0.7% with respect to the main edge jump is detected, confirming that the ground state contains a minor contribution of Co^{II}_{HS} in line with the XAS analysis of the ground state. After laser irradiation at 2 K, the magnetic state of Cs-Fe_4Co_4 is considerably modified as shown by the XMCD signals reported in **Figure 3a-b**. Indeed, a significant XMCD signal is detected from Fe^{III}_{LS} together with a strong XMCD contribution of Co^{II}_{HS}, leading to 21% and 50% of signal normalized to the main edge jump, respectively. The intensity of the XMCD is well reproduced by the calculations performed in C_{3v}

point symmetry for Fe^{3+} and Co^{2+} (note that we did not obtain any XMCD signal for the calculations described above while performed for Fe^{2+} and Co^{3+} in good agreement with their expecting low spin state). From the calculations of the XMCD signals, we extract for the Fe (respectively for the Co) the orbital angular kinetic momentum <Lz> = XX (resp. XX), the spin kinetic momentum <Sz> = XX (resp. XX) and the magnetic dipole <Tz> = XX (resp. XX). From the comparison of the experimental XMCD signal with the calculated ones with the magnetic field set along the C_{3v} axis one finds that the observed Co and Fe magnetic moments are both oriented parallel to the external magnetic field at 6.8 T. This clearly demonstrates the absence of a significant antiferromagnetic coupling between the metal ions in the paramagnetic excited state. In order to investigate further the magnetic coupling between the ions, we have obtained the field dependent magnetization for both Fe and Co from XMCD, as shown in **Figure 3c** in the paramagnetic excited state. Figure 3c shows a superposition of the element-specific magnetization curves M(H) which do not saturate at 6.8 T.This result contrasts with the previous studies which have demonstrated a strong antiferromagnetic coupling between Co and Fe in PBA 3D networks. Recently reported XMCD measurements of the dinuclear FeCo complex have led to similar conclusions. A ferromagnetic coupling cannot be excluded, however from the current set of data it is not possible to discriminate between a ferromagnetic Fe-Co exchange interaction and a paramagnetic behavior of the ions with their spins aligned along the direction of the magnetic field applied. Considering the Heisenberg-Dirac Hamiltonian $\widehat{H}^{spin} = -J.\vec{S}_{Fe}.\vec{S}_{Co}$.and by comparison with the temperature in the experiment we estimate a lower bound for the Fe-Co superexchange coupling of $J \gtrsim -0.5\ \mathrm{cm}^{-1}$. This can be interpreted in that a very weak antiferromagnetic coupling, no coupling or a ferromagnetic coupling are consistent with our observations. A strong antiferromagnetic coupling can be ruled out.

In summary, using L-edge XAS as an element-specific probe of the valence and spin states of Fe and Co ions in Cs-Fe_4Co_4 discrete molecular cubes we have observed directly the concurrent electronic and magnetic changes of both types of ions upon light irradiation. These results demonstrate beyond the shadow of doubt the existence of the light-induced ETCST process and its thermal relaxation in the molecular cages. The XMCD measurements directly reveal a ferromagnetic arrangement of the Fe and Co spins in the photoexcited state at 2 K for all applied magnetic field values. Furthermore, XMCD rules out the possibility of a strong antiferromagnetic coupling. Our study paves the way toward the integration of the present Cs-Fe_4Co_4 cages, featuring excellent photomagnetic properties and a high solubility, into organic electronics devices.

ASSOCIATED CONTENT

Supporting Information: Crystal field multiplet calculations; best-fit parameters of the LFM calculations; reference spectra of Fe and best fits; reference spectra of Co and best fits; best-fit calculated spectra of the ground state; best-fit calculated spectra of the paramagnetic excited state; time dependence of Fe^{III} and Co^{II} spectral features during laser irradiation.

ACKNOWLEDGMENTS

The authors thank Stefan Zeugin for his technical support during the experiments. Furthermore, the authors thank Marius Retegan for his help with the CRISPY software. Funding from the European Union's Horizon 2020 research and innovation programme under the Marie Skłodowska-Curie grant agreement No 701647 (M.S.) and from the Swiss National Science Foundation (grant nos. 200021_165774/1 and 200020_182599/1, M.S., N.D. and J.D.) is acknowledged.

REFERENCES

(1) Sato, O.; Tao, J.; Zhang, Y.-Z. Control of Magnetic Properties through External Stimuli. *Angew. Chem. Int. Ed.* **2007**, *46* (13), 2152–2187. https://doi.org/10.1002/anie.200602205.

(2) Li J.; Qiu J.-D.; Xu J.-J.; Chen H.-Y.; Xia X.-H. The Synergistic Effect of Prussian-Blue-Grafted Carbon Nanotube/Poly(4-vinylpyridine) Composites for Amperometric Sensing. *Adv. Funct. Mater.* **2007**, *17* (9), 1574–1580. https://doi.org/10.1002/adfm.200600033.

(3) Létard, J.-F.; Guionneau, P.; Goux-Capes, L. Towards Spin Crossover Applications. In *Spin Crossover in Transition Metal Compounds III*; Gütlich, P., Goodwin, H. A., Eds.; Topics in Current Chemistry; Springer Berlin Heidelberg: Berlin, Heidelberg, 2004; pp 221–249. https://doi.org/10.1007/b95429.

(4) Ricci, F.; Palleschi, G. Sensor and Biosensor Preparation, Optimisation and Applications of Prussian Blue Modified Electrodes. *Biosens. Bioelectron.* **2005**, *21* (3), 389–407. https://doi.org/10.1016/j.bios.2004.12.001.

(5) Karyakin, A. A.; Puganova, E. A.; Budashov, I. A.; Kurochkin, I. N.; Karyakina, E. E.; Levchenko, V. A.; Matveyenko, V. N.; Varfolomeyev, S. D. Prussian Blue Based Nanoelectrode Arrays for H2O2 Detection. *Anal. Chem.* **2004**, *76* (2), 474–478. https://doi.org/10.1021/ac034859l.

(6) Kahn, O.; Kröber, J.; Jay, C. Spin Transition Molecular Materials for Displays and Data Recording. *Adv. Mater.* **1992**, *4* (11), 718–728. https://doi.org/10.1002/adma.19920041103.

(7) Kahn, O.; Martinez, C. J. Spin-Transition Polymers: From Molecular Materials Toward Memory Devices. *Science* **1998**, *279* (5347), 44–48. https://doi.org/10.1126/science.279.5347.44.

(8) Keggin, J. F.; Miles, F. D. Structures and Formulæ of the Prussian Blues and Related Compounds. *Nature* **1936**, *137* (3466), 577–578. https://doi.org/10.1038/137577a0.

(9) Sato, O.; Iyoda, T.; Fujishima, A.; Hashimoto, K. Photoinduced Magnetization of a Cobalt-Iron Cyanide. *Science* **1996**, *272* (5262), 704.

(10) Tokoro, H.; Ohkoshi, S. Novel Magnetic Functionalities of Prussian Blue Analogs. *Dalton Trans.* **2011**, *40* (26), 6825. https://doi.org/10.1039/c0dt01829e.

(11) Bleuzen, A.; Lomenech, C.; Escax, V.; Villain, F.; Varret, F.; Cartier dit Moulin, C.; Verdaguer, M. Photoinduced Ferrimagnetic Systems in Prussian Blue Analogues CIxCo4[Fe(CN)6]y (CI = Alkali Cation). 1. Conditions to Observe the Phenomenon. *J. Am. Chem. Soc.* **2000**, *122* (28), 6648–6652. https://doi.org/10.1021/ja000348u.

(12) Berlinguette, C. P.; Dragulescu-Andrasi, A.; Sieber, A.; Galán-Mascarós, J. R.; Güdel, H.-U.; Achim, C.; Dunbar, K. R. A Charge-Transfer-Induced Spin Transition in the Discrete Cyanide-Bridged Complex {[Co(Tmphen)2]3[Fe(CN)6]2}. *J. Am. Chem. Soc.* **2004**, *126* (20), 6222–6223. https://doi.org/10.1021/ja039451k.

(13) Li, D.; Clérac, R.; Roubeau, O.; Harté, E.; Mathonière, C.; Le Bris, R.; Holmes, S. M. Magnetic and Optical Bistability Driven by Thermally and Photoinduced Intramolecular Electron Transfer in a Molecular Cobalt−Iron Prussian Blue Analogue. *J. Am. Chem. Soc.* **2008**, *130* (1), 252–258. https://doi.org/10.1021/ja0757632.

(14) Koumousi, E. S.; Jeon, I.-R.; Gao, Q.; Dechambenoit, P.; Woodruff, D. N.; Merzeau, P.; Buisson, L.; Jia, X.; Li, D.; Volatron, F.; et al. Metal-to-Metal Electron Transfer in Co/Fe

Prussian Blue Molecular Analogues: The Ultimate Miniaturization. *J. Am. Chem. Soc.* **2014**, *136* (44), 15461–15464. https://doi.org/10.1021/ja508094h.

(15) Garnier, D.; Jiménez, J.-R.; Li, Y.; Bardeleben, J. von; Journaux, Y.; Augenstein, T.; B. Moos, E. M.; T. Gamer, M.; Breher, F.; Lescouëzec, R. K⊂{[Fe II (Tp)(CN) 3] 4 [Co III (Pz Tp)] 3 [Co II (Pz Tp)]}: A Neutral Soluble Model Complex of Photomagnetic Prussian Blue Analogues. *Chem. Sci.* **2016**, *7* (8), 4825–4831. https://doi.org/10.1039/C6SC01435F.

(16) Li, D.; Parkin, S.; Wang, G.; Yee, G. T.; Clérac, R.; Wernsdorfer, W.; Holmes, S. M. An *S* = 6 Cyanide-Bridged Octanuclear Fe $^{III}{}_4$ Ni $^{II}{}_4$ Complex That Exhibits Slow Relaxation of the Magnetization. *J. Am. Chem. Soc.* **2006**, *128* (13), 4214–4215. https://doi.org/10.1021/ja058626i.

(17) Zhang Yuanzhu; Li Dongfeng; Clérac Rodolphe; Kalisz Marguerite; Mathonière Corine; Holmes Stephen M. Reversible Thermally and Photoinduced Electron Transfer in a Cyano-Bridged {Fe2Co2} Square Complex. *Angew. Chem.* **2010**, *122* (22), 3840–3844. https://doi.org/10.1002/ange.201000765.

(18) Mondal, A.; Li, Y.; Seuleiman, M.; Julve, M.; Toupet, L.; Buron-Le Cointe, M.; Lescouëzec, R. On/Off Photoswitching in a Cyanide-Bridged {Fe $_2$ Co $_2$ } Magnetic Molecular Square. *J. Am. Chem. Soc.* **2013**, *135* (5), 1653–1656. https://doi.org/10.1021/ja3087467.

(19) Shiga, T.; Tetsuka, T.; Sakai, K.; Sekine, Y.; Nihei, M.; Newton, G. N.; Oshio, H. Cyanide-Bridged Decanuclear Cobalt–Iron Cage. *Inorg. Chem.* **2014**, *53* (12), 5899–5901. https://doi.org/10.1021/ic500964m.

(20) Nihei, M.; Ui, M.; Hoshino, N.; Oshio, H. Cyanide-Bridged Iron(II,III) Cube with Multistepped Redox Behavior. *Inorg. Chem.* **2008**, *47* (14), 6106–6108. https://doi.org/10.1021/ic7024582.

(21) Cartier dit Moulin, C.; Villain, F.; Bleuzen, A.; Arrio, M.-A.; Sainctavit, P.; Lomenech, C.; Escax, V.; Baudelet, F.; Dartyge, E.; Gallet, J.-J.; et al. Photoinduced Ferrimagnetic Systems in Prussian Blue Analogues CIxCo4[Fe(CN)6]y (CI = Alkali Cation). 2. X-Ray Absorption Spectroscopy of the Metastable State. *J. Am. Chem. Soc.* **2000**, *122* (28), 6653–6658. https://doi.org/10.1021/ja000349m.

(22) Bleuzen, A.; Lomenech, C.; Dolbecq, A.; Villain, F.; Goujon, A.; Roubeau, O.; Nogues, M.; Varret, F.; Baudelet, F.; Dartyge, E.; et al. Photo-Induced Electron Transfer and Magnetic Switching in CoFe Cyanides: Study of the Metastable State. *Mol. Cryst. Liq. Cryst. Sci. Technol. Sect. Mol. Cryst. Liq. Cryst.* **1999**, *335* (1), 253–262. https://doi.org/10.1080/10587259908028870.

(23) Lee, J.-J.; Sheu, H.; Lee, C.-R.; Chen, J.-M.; Lee, J.-F.; Wang, C.-C.; Huang, C.-H.; Wang, Y. X-Ray Absorption Spectroscopic Studies on Light-Induced Excited Spin State Trapping of an Fe(II) Complex. *J. Am. Chem. Soc.* **2000**, *122* (24), 5742–5747. https://doi.org/10.1021/ja9943290.

(24) Jesús Luque, F.; Agnieszka Kowalik, I.; Pablo Prieto-Ruiz, J.; Ángel Niño, M.; Prima-García, H.; Manuel Romero, F.; Arvanitis, D.; Coronado, E.; Miranda, R.; Miguel, J. J. de. Magnetic Ordering in an (Fe 0.2 Cr 0.8) 1.5 [Cr(CN) 6] Prussian Blue Analogue Studied with Synchrotron Radiation Based Spectroscopies. *J. Mater. Chem. C* **2018**, *6* (30), 8171–8186. https://doi.org/10.1039/C8TC02879F.

(25) Sekine, Y.; Nihei, M.; Kumai, R.; Nakao, H.; Murakami, Y.; Oshio, H. X-Ray-Induced Phase Transitions by Selective Excitation of Heterometal Ions in a Cyanide-Bridged Fe–

Co Molecular Square. *Chem. Commun.* **2014**, *50* (31), 4050–4052. https://doi.org/10.1039/C3CC48820A.

(26) Jafri, S. F.; Koumousi, E. S.; Arrio, M.-A.; Juhin, A.; Mitcov, D.; Rouzières, M.; Dechambenoit, P.; Li, D.; Otero, E.; Wilhelm, F.; et al. Atomic Scale Evidence of the Switching Mechanism in a Photomagnetic CoFe Dinuclear Prussian Blue Analogue. *J. Am. Chem. Soc.* **2019**, *141* (8), 3470–3479. https://doi.org/10.1021/jacs.8b10484.

(27) Champion, G.; Escax, V.; Cartier dit Moulin, C.; Bleuzen, A.; Villain, F.; Baudelet, F.; Dartyge, E.; Verdaguer, M. Photoinduced Ferrimagnetic Systems in Prussian Blue Analogues C^{I}_{x} $Co_4[Fe(CN)_6]_y$ (C^{I} = Alkali Cation). 4. Characterization of the Ferrimagnetism of the Photoinduced Metastable State in $Rb_{1.8}Co_4[Fe(CN)_6]_{3.3}\cdot 13H_2O$ by K Edges X-Ray Magnetic Circular Dichroism. *J. Am. Chem. Soc.* **2001**, *123* (50), 12544–12546. https://doi.org/10.1021/ja011297j.

(28) Lescouëzec, R.; Vaissermann, J.; Ruiz-Pérez, C.; Lloret, F.; Carrasco, R.; Julve, M.; Verdaguer, M.; Dromzee, Y.; Gatteschi, D.; Wernsdorfer, W. Cyanide-Bridged Iron(III)–Cobalt(II) Double Zigzag Ferromagnetic Chains: Two New Molecular Magnetic Nanowires. *Angew. Chem. Int. Ed.* **2003**, *42* (13), 1483–1486. https://doi.org/10.1002/anie.200250243.

(29) Pardo, E.; Verdaguer, M.; Herson, P.; Rousselière, H.; Cano, J.; Julve, M.; Lloret, F.; Lescouëzec, R. Synthesis, Crystal Structures, and Magnetic Properties of a New Family of Heterometallic Cyanide-Bridged FeIII2MII2 (M = Mn, Ni, and Co) Square Complexes. *Inorg. Chem.* **2011**, *50* (13), 6250–6262. https://doi.org/10.1021/ic200616p.

(30) Jiménez, J.-R.; Tricoire, M.; Garnier, D.; Chamoreau, L.-M.; Bardeleben, J. von; Journaux, Y.; Li, Y.; Lescouëzec, R. A New {Fe4Co4} Soluble Switchable Nanomagnet Encapsulating Cs+: Enhancing the Stability and Redox Flexibility and Tuning the Photomagnetic Effect. *Dalton Trans.* **2017**, *46* (44), 15549–15557. https://doi.org/10.1039/C7DT02989F.

(31) Piamonteze, C.; Flechsig, U.; Rusponi, S.; Dreiser, J.; Heidler, J.; Schmidt, M.; Wetter, R.; Calvi, M.; Schmidt, T.; Pruchova, H.; et al. X-Treme Beamline at SLS: X-Ray Magnetic Circular and Linear Dichroism at High Field and Low Temperature. *J. Synchrotron Radiat.* **2012**, *19* (5), 661–674. https://doi.org/10.1107/S0909049512027847.

(32) Stavitski, E.; de Groot, F. M. F. The CTM4XAS Program for EELS and XAS Spectral Shape Analysis of Transition Metal L Edges. *Micron* **2010**, *41* (7), 687–694. https://doi.org/10.1016/j.micron.2010.06.005.

(33) Hocking, R. K.; Wasinger, E. C.; de Groot, F. M. F.; Hodgson, K. O.; Hedman, B.; Solomon, E. I. Fe L-Edge XAS Studies of K4[Fe(CN)6] and K3[Fe(CN)6]: A Direct Probe of Back-Bonding. *J. Am. Chem. Soc.* **2006**, *128* (32), 10442–10451. https://doi.org/10.1021/ja061802i.

(34) van der Laan, G.; Arenholz, E.; Chopdekar, R. V.; Suzuki, Y. Influence of Crystal Field on Anisotropic X-Ray Magnetic Linear Dichroism at the ${\mathrm{Co}}^{2+}$ ${L}_{2,3}$ Edges. *Phys. Rev. B* **2008**, *77* (6), 064407. https://doi.org/10.1103/PhysRevB.77.064407.

(35) Ridier, K.; Mondal, A.; Boilleau, C.; Cador, O.; Gillon, B.; Chaboussant, G.; Le Guennic, B.; Costuas, K.; Lescouëzec, R. Polarized Neutron Diffraction to Probe Local Magnetic Anisotropy of a Low-Spin Fe(III) Complex. *Angew. Chem. Int. Ed.* **2016**, *55* (12), 3963–3967. https://doi.org/10.1002/anie.201511354.

(36) Jafri, S. F.; Koumousi, E. S.; Arrio, M.-A.; Juhin, A.; Mitcov, D.; Rouzieres, M.; Dechambenoit, P.; Li, D.; Otero, E.; Wilhelm, F.; et al. Atomic Scale Evidence of the Switching Mechanism in a Photomagnetic CoFe Dinuclear Prussian Blue Analogue. *J. Am. Chem. Soc.* **2018**. https://doi.org/10.1021/jacs.8b10484.